Available online at www.sciencedirect.com
ScienceDirect
Journal of Power Sources 172 (2007) 225–228
JOURNAL OF POWER SOURCES
www.elsevier.com/locate/jpowsour

Short communication

Neutron images of the through-plane water distribution of an operating PEM fuel cell

D.S. Hussey [a,*], D.L. Jacobson [a], M. Arif [a], J.P. Owejan [b], J.J. Gagliardo [b], T.A. Trabold [b]

[a] *National Institute of Standards and Technology, 100 Bureau Dr., M.S. 8461, Gaithersburg, MD 20899-8461, USA*
[b] *General Motors Fuel Cell Activities, 10 Carriage Street, Honeoye Falls, NY 14472-0603, USA*

Received 25 April 2007; received in revised form 27 June 2007; accepted 3 July 2007
Available online 27 July 2007

Abstract

Neutron imaging has proven an invaluable tool for water metrology in operating proton exchange membrane fuel cells. Due to limitations in scintillator-based detector resolution, neutron imaging has been applied only to assessing the in-plane water distribution, without being able to distinguish water in the anode from the cathode. A new detector technology, based on micro-channel plates, enables a near order of magnitude improvement in the image resolution. This new detector technology will enable direct measurement of the through-plane water distribution in the gas diffusion layer, and enable the determination of the relative water content on the anode and cathode sides of a proton exchange membrane fuel cell. We report on the initial measurements with this new detector and discuss future measurement possibilities.

Keywords: Neutron imaging; Through-plane water distribution; Proton exchange membrane fuel cell; Gas diffusion layer

1. Introduction

Current state of the art neutron imaging is based on neutron scintillators, such ^{6}Li-doped ZnS [1]. For a typical scintillator thickness of 0.3 mm, there is an approximate 20% thermal neutron detection efficiency and a spatial resolution of $\Delta \approx 250$ μm. Here, spatial resolution is defined as 10% of the modulation transfer function (MTF), which is approximately the Rayleigh criterion [2]. There has been recent work to improve the spatial resolution in scintillators by investigating different binder materials and spatial resolutions reaching 50 μm have been reported, though the detection efficiency is reduced due to the required thinner scintillator [3]. However, even with a high-resolution scintillator, it would not be possible to image the through-plane water distribution in a proton exchange membrane (PEM) fuel cell and unambiguously distinguish the anode from the cathode in typical PEM materials. The resolution limitation is a result of the "light blooming", which is the scattering of the scintillation light in the scintillator and scales approximately with the scintillator thickness.

Recently, a micro-channel plate (MCP)-based counting detector has been demonstrated to have $\Delta \approx 25$ μm (10% MTF) with a thermal neutron detection efficiency of about 20% [4]. An MCP is a glass structure with straight-through, open channels with center-to-center separations of order 10 μm. The glass walls, typically a few micrometer thick are loaded with a neutron absorbing material, such as boron or gadolinium, which emits an energetic, charged particle as a result of the nuclear reaction. Two additional MCPs, which are not loaded with neutron absorber, are placed in series with the neutron MCP. A high voltage (about 5 kV) is applied across the entire MCP stack, which results in an electron avalanche with a charge amplification of about 10^{6}. (The non-neutron-sensitive MCPs provide sufficient charge amplification of the signal.) The position of the charge cloud, and hence the location of the neutron capture, is determined by a cross-delay line anode via centroiding with resolution of order a few micrometers. The resulting image resolution is then roughly twice the center-to-center channel separation. For currently available neutron-sensitive MCPs, the channel diameter is 10 μm, though there is research into neutron-sensitive MCP

* Corresponding author. Tel.: +1 301 975 6465; fax: +1 301 926 1604.
E-mail address: daniel.hussey@nist.gov (D.S. Hussey).

0378-7753/$ – see front matter © 2007 Elsevier B.V. All rights reserved.
doi:10.1016/j.jpowsour.2007.07.036

glass with smaller channel diameters, and in the future the technology may achieve an ultimate resolution of 10 μm [5]. A challenge of an MCP-based detector is that it requires a fast, event counting, electronic readout. Currently available readouts have a 1% dead time at a 200 kHz global count rate, and it is believed that higher rates are possible with cross-strip anodes, which are under development [6]. In practice, this upper limit to the event rate leads to a restriction of the field of view for a given neutron fluence rate.

To date, neutron imaging of PEM fuel cells has focused primarily on the in-plane water distribution due to the spatial resolution limitations of scintillators, although there has been some effort at tomography (three-dimensional images) and real-time through-plane radiography using thick (about 800 μm) gas diffusion layers (GDLs) [8] in order to just resolve anode GDL from cathode GDL. To obtain a fundamental understanding of the transport regimes so that accurate models can be developed, it is essential to measure the through-plane water distribution of the GDL and membrane electrode assembly (MEA). The current resolution of the MCP detectors will permit the investigation of the average water profile in the GDL for a particular set of operating parameters. This paper discusses initial efforts at visualizing the *in situ* through-plane water distribution of a PEM fuel cell using an MCP detector at the thermal neutron imaging facility at the NIST Center for Neutron Research [9].

2. Experimental design

The first consideration is to ensure that the experimental setup on the neutron beam line yields a geometric blur, λ_g, that is less than the detector's spatial resolution. Image formation in neutron radiography is well described by pinhole optics [2,7]. In pinhole optics one calculates λ_g as the minified image of the neutron source imaged through a point at the object plane using similar triangles:

$$\lambda_g = \frac{Dz}{L-z} \approx z\frac{D}{L}, \quad (1)$$

where D is the source aperture diameter ($D \approx 5$ mm), z the distance between the sample and detector, and L is the distance between the source and the detector ($L \approx 6$ m at the current NIST neutron imaging facility). The geometric blur describes how far two points must be separated in order to be resolved, and contributes, independently from the detector resolution, to the overall spatial resolution of a neutron image. Minimizing λ_g is crucial to utilize the new detector technology and yields two fuel cell design criteria: (1) the cell should be mounted as close to the detector as possible, and (2) to avoid blurring along the length of the cell, the thickness parallel to the beam axis should be minimized. An estimate of the image spatial resolution can be calculated by assuming the image formation process is linear, and all the point spread functions (blur and detector resolution) can be approximated by a simple Gaussian, in which case the resultant image resolution is

$$\delta = \sqrt{\lambda_g^2 + \Delta^2} \quad (2)$$

In this case, the midpoint of the cell was mounted approximately 2 cm from the detector surface, so that $\lambda_g \approx 17$ μm and $\delta \approx 30$ μm. As an aside, the image spatial resolution is a separate matter from the uncertainty in the measurement of the liquid water thickness. As outlined above, the spatial resolution is a function of the detector and the geometry on the beam line. The liquid water thickness resolution is related to Poisson counting statistics, and is a function of the neutron intensity. There is a tradeoff between spatial resolution, temporal resolution and liquid water thickness uncertainty that will be discussed in more detail in a future publication [10].

In order to meet the two design criteria, a PEM fuel cell was built with an active area 0.4 cm × 25 cm, with flow fields machined from aluminum (to reduce neutron scattering) with three channels that have a 1 mm period, 0.5 mm width, 0.3 mm depth, and 25 cm length. All aluminum surfaces were gold coated to prevent corrosion. The GDL consisted of Toray TGP-H-1.0 with 7% Teflon by weight applied [11] with an uncompressed thickness of about 1.0 mm. The membrane was Nafion 117, coated with a carbon–platinum catalyst, with a Pt areal density of 0.4 mg cm^{-2}. During operation, the cell was maintained at 80 °C using four cartridge heaters and active air cooling. In order to eliminate drifts in the cell position with respect to the detector, the cell was mounted directly to the detector face. In addition, to reduce the event rate, the inactive region of the cell was masked off with cadmium, except for a region used to normalize incident intensities, as shown in Fig. 1.

The unmasked region of the cell had a total area of approximately 1 cm^2, which corresponded to the center 2 cm of the cell length being imaged. The fluence rate of the 5 mm aperture was about 1×10^6 cm^{-2} s^{-1}, yielding a neutron event rate of approximately 200 kHz, which is in the regime where dead time corrections are negligible [4]. An exposure time of about 20 min was chosen so that there were on average 200 neutrons per pixel per image. In principle, a larger diameter aperture could be used to increase the fluence rate. (The dead time did not limit the integration time, merely the field of view that is possible

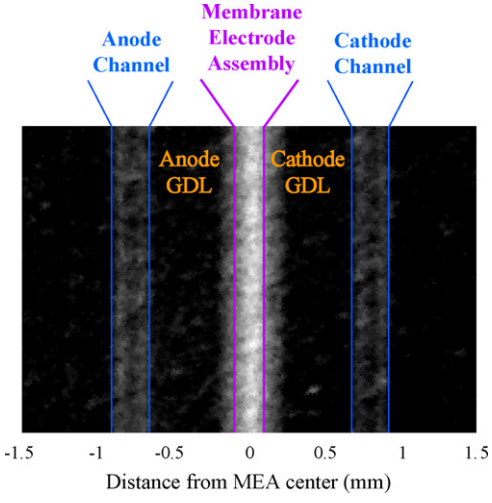

Fig. 1. A representative section of the change in water content image for the condition 100% RH, 0.2 A cm^{-2}. The main components of the cell are indicated. The corresponding water content is shown in Fig. 3.

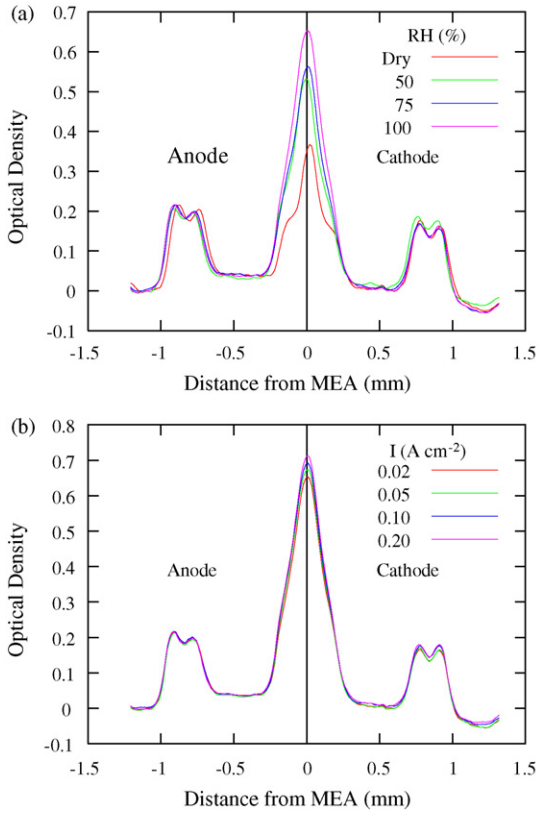

Fig. 2. Total optical density comparison with cell at 80 °C (a) at different relative humidities, at a current density of 0.02 A cm^{-2} compared to the dry state and (b) varying current densities at 100%.

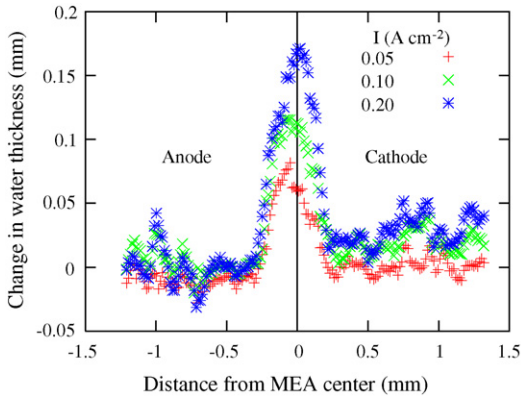

Fig. 3. The change in the through-plane water content at an RH of 100%, using as a reference state the current density at 0.02 A cm^{-2}. The center of the MEA was determined from Fig. 2b.

to expose to the full beam. Improvements in reducing the dead time would permit both larger fields of view, greater than 1 cm^2, as well as higher fluence rates. Higher fluence rates might be possible through changes to upstream neutron optical components that yield similar *L*/*D* ratios with higher intensities, such as reduction of Bi filter material [9].) In this case, if the image noise was due solely to simple Poisson counting statistics, the per pixel liquid water uncertainty would be about 0.3 mm. However, the detector electronics introduce additional noise, resulting in coarser liquid water thickness sensitivity. Since the final interest is the through-plane water distribution, averaging along the in-plane direction will decrease the uncertainty by the square root of the number of pixels averaged, provided the cell is truly one-dimensional. In the data shown in Figs. 2 and 3 a region 300 pixels wide was used to determine the water distribution, and had an image derived standard deviation of the liquid water thickness of about 50 μm. Further reduction in this uncertainty is possible, for instance through longer image integration times.

3. Results

The cell was operated in counter flow, so as to ensure the highest water concentration at the center of the cell which was in the field of view of the detector, as opposed to running in co-flow which could result in a higher concentration of liquid water at the outlet. The anode (pure hydrogen) and cathode (air) inlet gases were maintained at the same humidities, with constant flow rates for the anode and cathode of about 695 sccm and 1665 sccm, respectively, for all conditions, with no channel water observed in the images (see Table 1 for operating conditions). The high flow rate was used to eliminate any water slug formation in the channels. The cell was maintained at an absolute pressure of about 110 kPa. The cell was operated at a relative humidity (RH) of 50%, 75% and 100% at a current density of 0.02 A cm^{-2}. Additionally, operating points were obtained in the kinetic region at an RH of 100% at current densities of 0.02 A cm^{-2}, 0.05 A cm^{-2}, 0.01 A cm^{-2} and 0.2 A cm^{-2}, and the cell performance is summarized in Table 1. The study focused on low current densities because in this operating regime, reactant flow in the channels is insufficient to mitigate by convection GDL water accumulation. Additionally, for many practical applications, including automotive propulsion, the majority of fuel cell operation occurs at low current density (less than 20% maximum).

An unanticipated image analysis complication came from the swelling of the membrane, which resulted in a total motion of about 50 μm for Nafion 117. The swelling is evident in Fig. 2a in comparing the location of the boundary of the anode GDL and the channels, which is the rise at about 700 μm from the center of the MEA assembly. The motion complicates the analysis since typically one applies the Lambert–Beer law of attenuation to determine the liquid water thickness, using a dry image of the cell as the reference image. Since the membrane swelled and potentially displaced the flow fields asymmetrically as the cell was mounted to the detector face meaning there was no reference surface, the simple Lambert–Beer's law analysis will not

Table 1
Summary of the test section's performance and stoichiometric ratios at anode and cathode inlet RH of 100%

I (A cm^{-2})	Voltage (V)	Anode stoich	Cathode stoich
0.023 ± 0.001	0.7245 ± 0.0007	437 ± 21	440 ± 21
0.052 ± 0.001	0.667 ± 0.001	189 ± 4	191 ± 3
0.1023 ± 0.0009	0.579 ± 0.003	97.0 ± 1.0	97.7 ± 0.9
0.202 ± 0.001	0.423 ± 0.003	49.0 ± 0.3	49.4 ± 0.3

The uncertainties represent ±1S.D. of the measured value during the 20 min exposure time.

produce meaningful results. In other words, quantifying the total liquid water content would require approximations which may or may not hold, and so cannot be inferred from these images. However, two analysis approaches could be taken, one forming the total optical density of the cell using a flat field (see Fig. 2), and the other by looking at the change in water content during the polarization curve (see Fig. 3).

Shown in Fig. 2a is a comparison of the optical densities at a temperature of 80 °C, 0.02 A cm^{-2} for an RH of 50%, 75% and 100%. The swelling is a reversible process, as the order of the conditions corresponding to Fig. 2 were 75% RH, 100% RH (and then the polarization curve, conditions shown in the inset of Fig. 2b), cell purge and dry out, and finally 50% RH. Since the channels are gold coated, the bottom of the channels and the lands present a thick layer of gold to the neutron beam, and thus a higher optical density. This gives rise to the two small peaks in Fig. 2a about 1.0 mm from the MEA. The MEA center was located by assuming it was equidistant from the anode and cathode lands.

Since the membrane was in a constant location during the polarization curve, it is straight-forward to look at the change in water content as the current density is increased, using as the reference state the current density of 0.02 A cm^{-2}, in a manner similar to that performed in Ref. [13]. Due to the shifts that have occurred, registering the location of the cell components has uncertainty that is difficult to assess. However, the images demonstrate that the water content in the anode GDL remains fairly constant, while there appears to be a slight build-up of water in the cathode GDL as the cell produces more current. Additionally, the water content of the membrane increases with higher current as well.

4. Conclusions and future plans

We have demonstrated the visualization of the through-plane water distribution with a spatial resolution of 30 μm with neutron imaging. The analysis suffered from the ability to resolve the membrane swelling, and future work will focus on mitigating this problem. For instance, thinner membranes will have a smaller total volume change, reducing the problem. Additionally, rather than being directly coupled to the detector, the cell will be mounted from the bottom, providing a reference surface for determining the location of cell components. Further, a gage can be placed on the cell to provide an accurate measurement of the distances in the image. We believe the ongoing development of neutron MCP detectors will reach an ultimate resolution of about 10 μm.

Acknowledgments

This work was supported by the U.S. Department of Commerce, the NIST Ionizing Radiation Division, the Director's Office of NIST, the NIST Center for Neutron Research, and the Department of Energy through interagency agreement no. DE-AI01-01EE50660.

References

[1] A.J. Spowart, NIM 75 (1969) 35–42.
[2] E. Hecht, Optics, Addison Wesley Longman Inc., Reading, MA, 1998.
[3] E.H. Lehmann, NIMA 576 (2007) 389–396.
[4] O.H.W. Siegmund, et al., NIMA 579 (2007) 188–191.
[5] W.B. Feller, et al., Proceedings of the 8th World Conference on Neutron Radiography, Gaithersburg, MD, USA, October 18, 2006.
[6] O.H.W. Siegmund, et al., Proceedings of the 8th World Conference on Neutron Radiography, Gaithersburg, MD, USA, October 18, 2006.
[7] H.H. Barrett, W. Swindell, Radiological Imagining, Academic Press, San Diego, CA, 1981.
[8] D.S. Hussey, et al., Proceedings of the 8th World Conference on Neutron Radiography, Gaithersburg, MD, USA, October 18, 2006.
[9] D.S. Hussey, et al., NIMA 542 (2005) 9–15.
[10] D.S. Hussey, et al., Conference Proceedings of the 2007 American Society of Mechanical Engineers Conference in New York, NY, June 18, 2007, submitted.
[11] Certain trade names and company products are mentioned in the text or identified in an illustration in order to adequately specify the experimental procedure and equipment used. In no case does such identification imply recommendation or endorsement by the National Institute of Standards and Technology, nor does it imply that the products are necessarily the best available for the purpose.
[13] M.A. Hickner, et al., JECS 153 (2006) A902–A908.